PASSIVE SHOCK CONTROL IN TRANSONIC FLOW FIELD

S. Matsuo[1*], M. Tanaka[1], T. Setoguchi[1], H. Kashimura[2], T. Yasunobu[2] and H. D. Kim[3]

In order to control the transonic flow field with a shock wave, a condensing flow was produced by an expansion of moist air on a circular bump model and shock waves were occurred in the supersonic parts of the fields. Furthermore, the additional passive technique of shock-boundary layer interaction using the porous wall with a cavity underneath was adopted in this flow field. The effects of these methods on the shock wave characteristics were investigated numerically. The result showed that the flow fields might be effectively controlled by the suitable combination between non-equilibrium condensation and the position of porous wall.

Keywords: Compressible Flow, Non-Equilibrium Condensation, Boundary Layer, Flow Control

1. INTRODUCTION

The transonic flow over the airfoil is characterized by a shock wave standing on the suction surface. In this case, the interaction between the shock wave and boundary layer becomes complex because the shock wave imposes an adverse pressure gradient on the boundary layer. Passive control technique using a porous wall and cavity system, when it is applied at the foot of the shock wave, is known to be effective in alleviating undesirable adverse pressure gradient of the shock wave-boundary layer interaction.[1,2] However, this control method essentially leads to large viscous losses caused by the porous walls, which can overcompensate the control benefit of the shock wave.

In recent years, possibilities for the control of flow fields due to non-equilibrium condensation have been clarified experimentally and numerically. [3,4] It is found from these works that when nonequilibrium condensation occurs in a supersonic nozzle, displacement thickness of boundary layer becomes thin behind the condensation zone. Furthermore, the development of boundary layer is reduced behind the shock wave and non-quilibrium condensation is effective to the reduction of high frequency components for oscillation of shock wave especially. Therefore, it is expected that the reduction of Mach number due to non-equilibrium condensation just before shock wave suppresses the separation of boundary layer generated by shock wave, and droplets generated by condensation suppress the fluctuation of flow field due to the shock wave instability.

In the present study, in order to control the transonic flow field with shock wave, a condensing flow is produced by an expansion of moist air in the nozzle with a circular bump model and shock waves are occurred in the supersonic parts of the flow fields. Furthermore, the additional passive technique of shock-boundary layer interaction using the porous wall with a cavity is adopted in this flow field. Computation is conducted to investigate the effectiveness of this kind of control techniques.

Received: July 12, 2004, Accepted: February 12, 2005.

1 Dept. of Mechanical Engineering, Saga University, 1 Honjo-machi, Saga-shi, Saga 840-8502, Japan.

2 Dept. of Control and Information Systems Engineering, Kitakyushu National College of Technology, 5-20-1, Shii, Kokuraminami-ku, Kitakyushu-shi, Fukuoka 802-0985.

3 School of Mechanical Engineering, College of Natural Science, Andong National University, 388, Songchung-dong, Andong 760-749, Korea.

* Corresponding author. Email: matsuo@me.saga-u.ac.jp

2. COMPUTATIONAL ANALYSIS

2.1 GOVERNING EQUATIONS

Like conventional two-phase flow analysis, several of assumptions were made for the present computations. There is no velocity slip and no temperature difference between condensate particles and medium gas flows, and due to very

small condensate particles the effect of the particles on pressure field can be neglected within the accuracy of the present computations.

The governing equations are unsteady two-dimensional, compressible, Navier-Stokes equations and a droplet growth equation[5] written in the Cartesian coordinate system (x, y). The governing equations were non-dimensionalized using the reference values at nozzle inlet conditions and are written as[5] ;

$$\frac{\partial \boldsymbol{Q}}{\partial t}+\frac{\partial \boldsymbol{E}}{\partial x}+\frac{\partial \boldsymbol{F}}{\partial y}=\frac{1}{\mathrm{Re}}\left(\frac{\partial \boldsymbol{R}}{\partial x}+\frac{\partial \boldsymbol{S}}{\partial y}\right)+\boldsymbol{H}, \tag{1}$$

where

$$\boldsymbol{Q}=\begin{bmatrix}\rho_m\\ \rho_m u\\ \rho_m v\\ \rho_m E_t\\ \rho_m g\\ \rho_m D_1\\ \rho_m D_2\\ \rho_m D_3\end{bmatrix},\ \boldsymbol{E}=\begin{bmatrix}\rho_m u\\ \rho_m u^2+p\\ \rho_m uv\\ u(E_t+p)\\ \rho_m ug\\ \rho_m uD_1\\ \rho_m uD_2\\ \rho_m uD_3\end{bmatrix},\ \boldsymbol{F}=\begin{bmatrix}\rho_m v\\ \rho_m uv\\ \rho_m v^2+p\\ v(E_t+p)\\ \rho_m vg\\ \rho_m vD_1\\ \rho_m vD_2\\ \rho_m vD_3\end{bmatrix},$$

$$\boldsymbol{R}=\begin{bmatrix}0\\ \tau_{xx}\\ \tau_{xy}\\ \alpha\\ 0\\ 0\\ 0\\ 0\end{bmatrix},\ \boldsymbol{S}=\begin{bmatrix}0\\ \tau_{yx}\\ \tau_{yy}\\ \beta\\ 0\\ 0\\ 0\\ 0\end{bmatrix},\ \boldsymbol{H}=\begin{bmatrix}0\\ 0\\ 0\\ 0\\ \rho_m\dot{g}\\ \rho_m\dot{D}_1\\ \rho_m\dot{D}_2\\ \rho_m\dot{D}_3\end{bmatrix}, \tag{2}$$

$$\alpha=u\tau_{xx}+v\tau_{yx}+\frac{\mu}{(\gamma-1)\mathrm{Pr}}\frac{\partial T}{\partial x},$$

$$\beta=u\tau_{xy}+v\tau_{yy}+\frac{\mu}{(\gamma-1)\mathrm{Pr}}\frac{\partial T}{\partial y}. \tag{3}$$

In these equations, ρ is the density. u and v are the Cartesian velocity components and g (ratio of condensate mass to total mass of the mixture) is condensate mass fraction. τ_{xx}, τ_{xy}, τ_{yx} and τ_{yy} are components of viscous shear stress. Subscript m refers to the mixture. g (condensate mass fraction), E_t (the total energy per unit mass) and p (pressure) are calculated by the following equations.

$$g=\frac{m_l}{m_a+m_v+m_l}, \tag{4}$$

$$E_t=\rho_m C_{p0}T+\frac{1}{2}\rho_m(u^2+v^2)-\rho_m gL, \tag{5}$$

$$p=G\left[E_t-\frac{1}{2}\rho_m\left(u^2+v^2\right)+\rho_m gL\right], \tag{6}$$

$$G=\left(1-g\frac{M_m}{M_v}\right)\Big/\left(\frac{1}{\gamma-1}+g\frac{M_m}{M_v}\right). \tag{7}$$

In the above equations, L (latent heat of condensation) is given by

$$L=L_0+L_1T\ (\mathrm{J/Kg}),\ L_0=3105913.39,$$
$$L_1=-2212.97\times10^{-2}, \tag{8}$$

where m is the mass flow rate, subscript a, v and l refer to air, vapour and liquid, respectively, C_p is specific heat at constant pressure, M is molecular weight.

$\dot{g}$, $\dot{D}_1$, $\dot{D}_2$ and $\dot{D}_3$ [5] in Eq.(2) are given by

$$\dot{g}=\frac{dg}{dt}=\frac{\rho_l}{\rho_m}\left(\frac{4\pi}{3}r_c^3I+\rho_m D_1\frac{\partial r}{\partial t}\right), \tag{9}$$

$$\dot{D}_1=\frac{dD_1}{dt}=\frac{4\pi r_c^2 I}{\rho_m}+D_2\frac{dr}{dt}, \tag{10}$$

$$\dot{D}_2=\frac{dD_2}{dt}=\frac{8\pi r_c I}{\rho_m}+D_3\frac{dr}{dt}, \tag{11}$$

$$\dot{D}_3=\frac{dD_3}{dt}=\frac{8\pi I}{\rho_m}. \tag{12}$$

In the above equations, nucleation rate I[6] that is the number of critical-size droplets formed per unit time per unit volume is given as follows ;

$$I=\frac{1}{\rho_l}\left(\frac{p_v}{kT}\right)^2\sqrt{\frac{2\sigma m_v}{\pi}}\exp\left\{\frac{-4\pi\sigma r_c^2}{3kT}\right\}, \tag{13}$$

and critical radius of the nuclei r_c and radius growth rate $\dot{r}$ [7] are

$$r_c=\frac{2\sigma}{\rho_l\Re T\ln(p_l/p_\infty)}, \tag{14}$$

$$\dot{r}=\frac{dr}{dt}=\frac{1}{\rho_l}\frac{p_v-p_{s,r}}{\sqrt{2\pi\Re T}}, \tag{15}$$

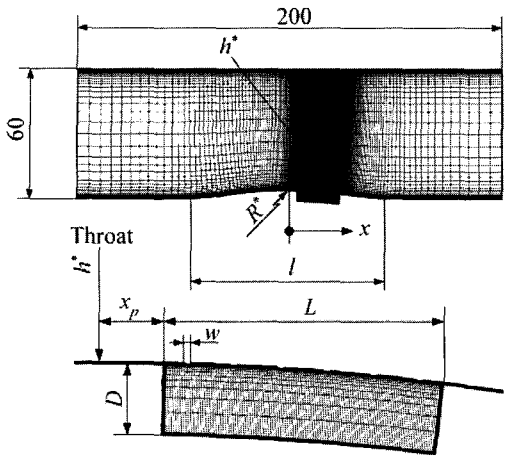

Fig. 1 Computational grid (Unit: mm)

$$p_{s,r} = p_\infty \exp\left(\frac{2\sigma}{\rho_l \Re T r}\right), \tag{16}$$

respectively. $\Re$ and k are gas constant and Boltzmann constant, respectively.

Density of water ρ_l, surface tension of vapor σ and saturated vapor pressure of equilibrium flat film p_∞ are

$$\rho_l = \begin{cases} \left(A_0 + A_1 t + A_2 t^2 + A_3 t^3 + A_4 t^4 + A_5 t^5\right)/\left(1 + B_0 t\right) \\ \qquad for \quad T \geq 0°C \\ \left(A_6 + A_7 t + A_8 t^2\right) \quad for \quad T < 249.39K \end{cases} \tag{17}$$

$$\begin{aligned} &A_0 = 999.8396, A_1 = 18.224944, \\ &A_2 = -7.92221\times10^{-3}, A_3 = -55.44846\times10^{-6}, \\ &A_4 = 149.7562\times10^{-9}, A_5 = -393.2952\times10^{-12} \\ &A_6 = 999.84, A_7 = 0.086, A_8 = -0.0108, \\ &B_0 = 18.159725\times10^{-3} \end{aligned} \tag{18}$$

$$\sigma = \begin{cases} \{76.1 + 0.155\times(273.15 - T)\}\times10^{-3} \\ \qquad for \quad T \geq 249.39K \\ \{\left(1.1313 - 3.7091\times10^{-3}\times T\right)\times10^{-4} \\ -5.6464\}\times10^{-6} \quad for \quad T < 249.39K \end{cases} \tag{19}$$

$$p_\infty = \exp\left(A_9 + A_{10}T + A_{11}T^2 + B_1 \ln(T) + \frac{C_0}{T}\right) \tag{20}$$

A_9=21.215,A_{10}=-2.7346x10^{-2},A_{11}=1.6853 x 10^{-5}

B_1=2.4576, C_0=-6094.4642, (21)

respectively.[8]

In the present study, governing systems were mapped from the physical plane of reference (x, y) into a computational plane of reference with a general transformation. To close the governing equations, Baldwin-Lomax model[9] was employed in computations. A third-order TVD (Total Variation Diminishing) finite difference scheme with MUSCL[10] was used to discretize the spatial derivatives, and a second order-central difference scheme for the viscous terms. A second-order fractional step was employed for time integration. The validity of the method used in the present calculation is shown in the previous researches.[11,12]

2.2 NUMERICAL CONDITIONS

Fig. 1 shows a computational grid of transonic nozzle flow field. A fine structured grid was used to capture the condensation shock waves. The number of grid points for the part of nozzle is 251 × 61 and 133 × 16 for the part of cavity. The nozzle has a height of 60 mm at the inlet and exit, a radius of circular arc R* =100 mm and a height of nozzle throat h*=56 mm. The bump wall surface consists of two-dimensional slots, having the cavity of a dimension L (=20 mm) × D (=5 mm). A cavity on the bump wall has a slot wall. The width of opening area between slots is constant at w=0.6 mm. Hereafter, the slotted wall is denoted as a porous wall. The porosity (the value of the total area of the slots divided by the surface area of the porous plate) of the porous wall is 0.18. x_p denotes the distance from nozzle throat to the leading edge of the cavity. Cases of R11 and R12 correspond to x_p=-3 mm and -5 mm, respectively. R1S is the case without the porous wall (solid wall). The initial degree of supersaturation S_{01} defined as the value of the ratio of vapour partial pressure p_{v01} and saturated vapour pressure p_{s01} in the reservoir is given as follows :

$$S_{01} = \frac{p_{v01}}{p_{s01}} \tag{22}$$

Values of the initial degree of supersaturation S_{01} and total temperature in the reservoir were set at 0.5 and 298 K, respectively. Total pressure in the reservoir was set at 102 kPa.

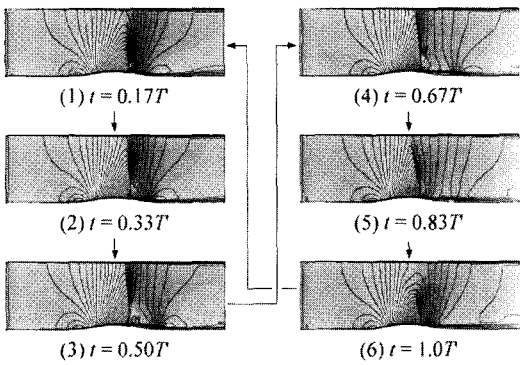

(a) Computer schlieren pictures

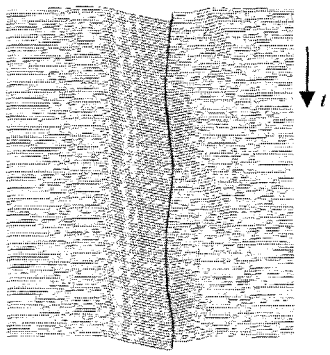

(b) Pressure diagram in flow field

Fig. 2 Schematic view of flow field oscillation (R1S, S_{01}=0)

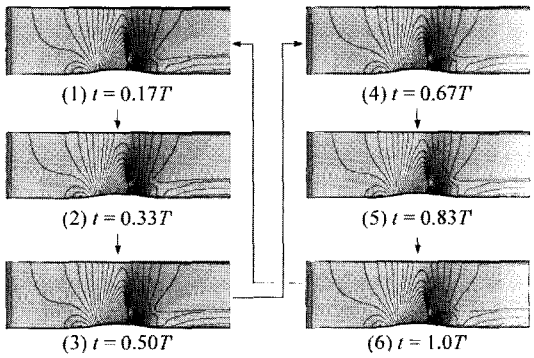

Fig. 3 Computer schlieren pictures (R1S, S_{01}=0)

3. RESULTS AND DISCUSSIONS

Fig. 2 shows computer schlieren pictures and time histories of static pressure distributions on a line close to the outer edge of boundary layer for the case of R1S (solid wall) without non-equilibrium condensation (S_{01}=0). In Fig. 2(a), computer schlieren pictures are shown during one cycle of flow oscillation (f = 669 Hz). Fig. 2(b) shows time histories of static pressure distributions on a line close to the outer edge of boundary layer. Here, T denotes the time of one cycle of oscillation. As seen from both figures, a shock wave oscillates periodically on the bump wall.

Fig. 3 shows computer schlieren pictures for R1S with non-equilibrium condensation (S_{01}=0.5). From this figure, it is found that the flow oscillation is suppressed effectively by non-equilibrium condenstion and the shock strength becomes weak in comparison with Fig. 2(a).

Fig. 4(a) and (b) show the contour maps of condensate mass fraction g and nucleation rate I corresponding to the numerical condition of Fig.3, respectively. Dotted lines denote the sonic line. It is found from Fig. 4(a) that condensate mass fraction increases rapidly on bump wall side upstream of the shock wave and distributes over downstream range. In Fig. 4(b), a large number of condensate nuclei generate on bump wall side and the distribution expands over both of solid boundaries.

Fig. 5(a) and (b) show computer schlieren pictures and time histories of static pressure distributions on a line close to the outer edge of boundary layer for the case of R11 (porous wall) without non-equilibrium condensation (S_{01}=0), respectively. Wavelets can be observed on the porous wall and the suppression of flow oscillation

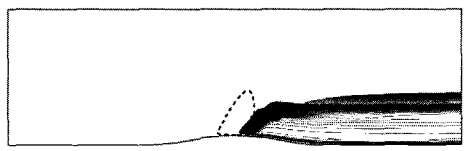

(a) Condensate mass fraction

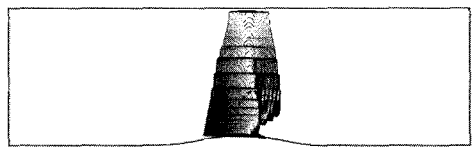

(b) Nucleation rate

Fig. 4 Contour maps of condensate properties (R1S, S_{01} = 0.5)

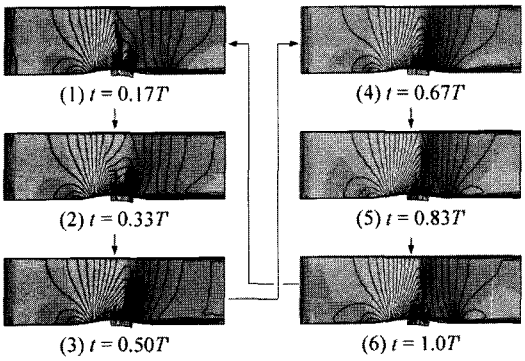

(a) Computer schlieren pictures

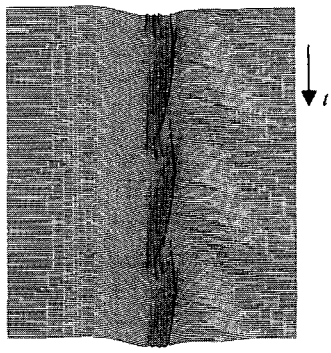

(b) Pressure diagram in flow field

Fig.5 Schematic view of flow field oscillation (R11, S_{01}=0)

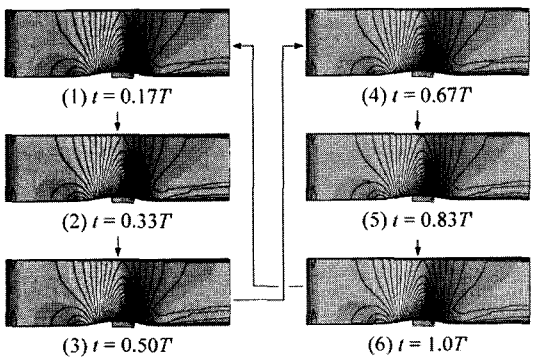

Fig.6 Computer schlieren pictures (R12, S_{01}= 0)

is not confirmed for this case. Furthermore, it was not also confirmed for the cases with non-equilibrium condensation (R11, S_{01}=0.5) and R12 without non-equilibrium condensation.

Fig. 6 shows computer schlieren pictures for the case of R12 (porous wall) with non-equilibrium condensation (S_{01}=0.5). It is found from this figure that the flow oscillation is nearly suppressed effectively.

Table 1 shows the frequency of flow field oscillation on a position of the porous wall. Cases of R1S are shown for reference. For the case without non-equilibrium condensation, flow oscillations are slightly reduced in cases with the porous wall (R11, R12). For R11 with non-equilibrium condensation, the frequency is almost the same as the case without non-equilibrium condensation. The oscillation of flow fields for R1S and R12 is suppressed in the case with non-equilibrium condensation. As a result, it is found that the suppression of flow oscillation might be effectively attained by the suitable combination between non-equilibrium condensation and the position of porous wall.

Fig. 7 shows variations of boundary layer displacement thickness of boundary layer δ_1 on the bump wall for cases of R1S and R12 with non-equilibrium condensation. Displacement thickness for R12 behind the separation is larger than that of R1S. This is due to blowing to main flow from the cavity inside upstream of the foot of the shock wave.

Fig. 8 shows distributions of total pressure loss (1- p_0/p_{01}) (p_0: local total pressure) along y - direction at the position of x/l = 0.4 (x = 22.4 mm) for cases of R1S and R12 with non-equilibrium condensation. For case of solid wall, total pressure loss with condensation in the main flow (y/l = 0.100 ~ 0.265) becomes larger than the case of R12 with condensation. However, total pressure loss on the bump wall side becomes small due to the suppression of boundary layer separation. For porous wall with condensation, total pressure loss on the bump wall side is slightly large in comparison with solid wall, and decreases in the main flow (y/l = 0.0769 ~ 0.276).

Table. 1 Frequencies of flow field oscillation

	R1S	R11	R12
S_{01} = 0	669 Hz	580 Hz	571 Hz
S_{01} = 0.5	—	579 Hz	—

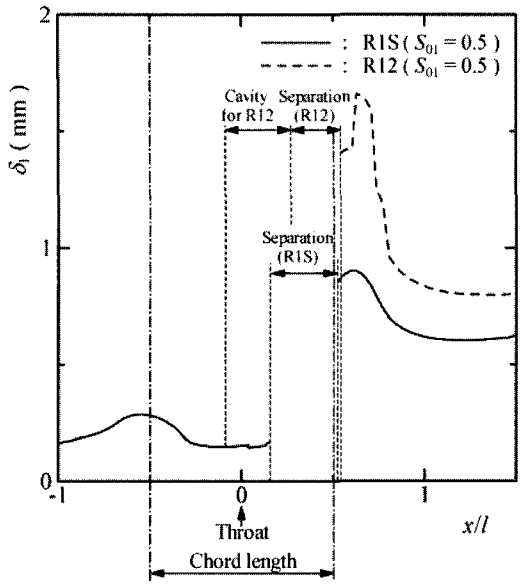

Fig. 7 Distributions of displacement thickness

Table 2 Total pressure loss (S_{01}=0.5)

R1S	R12
100 %	111 %

Total pressure losses in case with non-equilibrium condensation were integrated from the wall surface to the center (y = 30 mm) of the main flow at the position (x = 22.4 mm) as shown in Fig.8. Table 2 shows the ratio of integrated total pressure loss of R12 to the integrated total pressure loss for solid wall. As seen from this table, the ratio in case with non-equilibrium condensation for the porous wall (R12) becomes larger than the case of solid wall (R1S) with non-equilibrium condensation. As a result, in the point of view of suppression of flow oscillation and total pressure loss, it is important that the non-equilibrium condensation occurs in the flow field with the solid wall.

4. CONCLUSIONS

Computations were carried out to investigate the effects of the porous wall with a cavity underneath and non-equilibrium condensation on the transonic flow field with shock wave on the bump wall. The

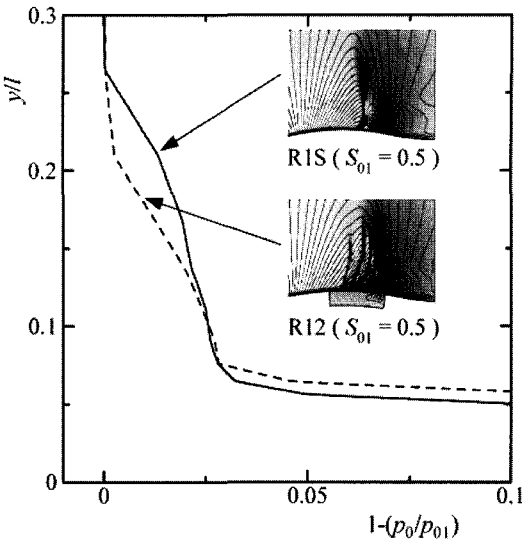

Fig. 8 Distributions of total pressure loss

present computation was very effective to obtain qualitative aspects of the flow filed. It was also found that the flow fields might be effectively controlled by the suitable combination between non-equilibrium condensation and the position of the porous wall.

REFERENCES

[1] Bahi, L., Ross, J.M. and Nagamatsu, H.T., 1983, "Passive Shock Wave/Boundary Layer Control for Transonic Airfoil Drag Reduc-tion," *AIAA 83-0137.*

[2] Raghunathan, S.R., 1988, "Passive Control of Shock-Boundary Layer Interaction," *Prog. Aerospace Sci.*, Vol.25, pp.271-296.

[3] Setoguchi, T., Matsuo, S., Yu, S. and Hirahara, H., 1997, "Effect of Nonequilibrium Homogeneous Condensation on Flow Fields in a Supersonic Nozzle," *Journal of Thermal Science,* Vol.6, No.2, pp.90-96.

[4] Matsuo, S., Setoguchi, T., Yu, S. and Matsuo, K., 1997, "Effect of Nonequilibrium Condensation of Moist Air on the Boundary Layer in a Supersonic Nozzle," *J. of Thermal Science,* Vol.6, No.4, pp.260-272.

[5] Sislian, J.P., 1975, "Condensation of Water Vapor with or without a Carrier Gas in a Shock Tube," *UTIAS Report,* No.201.

[6] Frenkel, J., 1945, *Kinetik der Phasenbildung*, Edwards Brothers.

[7] Mundinger, G., 1994, "Numerische Simulation instatinärer Lavaldüsenströmungen mit Energiezufuhr durch homogene Kondensation," Karlsruhe Universität.

[8] Adam, S., 1996, "Dissertation, Fakultät für Maschinenbau," Universität Karlsruhe (TH), Germany.

[9] Baldwin, B.S. and Lomax, H., 1978, "Thin layer approximation and algebraic model for separated turbulent flows," *AIAA paper,* No.78-257.

[10] Yee, H.C., 1989, "A class of high-resolution explicit and implicit shock-capturing methods," *NASA TM-89464.*

[11] Setoguchi, T., Matsuo, S., Shimamoto, K., Yu, S. and Kim, H.D., 2001, "Control of Condensation Shock Wave Using a Double Slot," *Proc. of 5th International Symposium on Experimental and Computational Aerothermodynamics of Internal Flows*, pp.461-468.

[12] Tanaka, M., Matsuo, S., Setoguchi, T., Kaneko, K., Kim, H.D. and Yu, S., 2003, "Passive Control of Transonic Flow Fields with Shock Wave Using Non-equilibrium Condensation and Porous wall," *Proc. of 6th International Symposium on Experimental and Computational Aerothermodynamics of Internal Flows,* Vol.1, pp.250-255.